Transport at a complex multiple-input-multiple-output TASEP junction

Asma Ben Janete, Partho Sakha De, Adélaïde Raguin

Physica A 693 (2026) 131466

Contents lists available at ScienceDirect

Physica A

journal homepage: www.elsevier.com/locate/physa

Transport at a complex multiple-input-multiple-output TASEP junction

Asma Ben Janete [a], Partho Sakha De [a], Adélaïde Raguin [a,b,*]

[a] Institute for Computational Cell Biology, Computer Science Department, Heinrich Heine University, Universitätsstr. 1, Düsseldorf, 40225, NRW, Germany

[b] Laboratoire Bordelais de Recherche en Informatique (LaBRI - UMR 5800), CNRS, Univ. Bordeaux, Bordeaux INP, Talence, 33405, France

ARTICLE INFO

Dataset link: https://gitlab.com/asben100/complex-tasep-mimo-junction

Keywords:
TASEP
Junction
Transport
Multiple-input-multiple-output
Constrained optimisation
Gillespie algorithm

ABSTRACT

The Totally Asymmetric Simple Exclusion Process (TASEP) is widely used to study transport on networks. Here, we focus on a multiple-input-multiple-output (MIMO) junction with complex kinetic rules and develop an innovative numerical method to solve the equation for mean-field current conservation at the junction using Constrained Optimisation, that we supplement with stochastic simulations following a Gillespie algorithm. We observe that lattices with the same ratio of upstream to downstream segments have the same phase diagrams, in the absence of bias, and in the absence of bottleneck effect. As soon as a bias is introduced on the side of the junction with fewer segments, a bottleneck effect arises, leading to a reduction of the current on the segments and at the junction, and a change of the junction current–density relation from quadratic to piece-wise quasi-linear. In the absence of bias, the bottleneck effect arises in particular in lattices where the rates of absorption into and pumping out of the junction lie under a certain threshold, which is dependent on the number of upstream and downstream segments, as well as the junction density. As biases are introduced on either or both of the upstream and downstream segments, a very complex phenomenology emerges on the overall lattice, involving a combinatorial explosion of the phases. Furthermore, particle–hole symmetry, well-established for a simple TASEP segment, extends here as well, enabling us to recover the phase diagrams for lattices with opposite configurations.

1. Introduction

The Totally Asymmetric Simple Exclusion Process (TASEP) is a widely used and studied stochastic transport model, which, in its simplest form, describes the unidirectional motion along a segment, of a gas of particles interacting as hard spheres [1]. In 1968, it was first introduced to depict the translation of mRNAs into proteins by ribosome-like hard-sphere particles [2–5]. Since then, thanks to its simplistic dynamic rules, TASEP has been extensively used to model many systems in diverse application fields, such as the movement of motor proteins along the cytoskeleton of eukaryotic cells [6–12], or that of pedestrians on sidewalks [13,14]. For instance, in the traffic flow theory, it enables evaluating the impact of pedestrians' walking rhythm and velocity, as well as transport policy and planning, thereby improving safety, comfort, and congestion, together with reducing cost and emissions [15–18].

TASEP on a single segment is a very simple system, whose exact solution can be obtained with the Bethe-Ansatz technique, and remarkably be recovered in the mean-field approximation while considering the thermodynamic limit [19,20]. Transport along branched lattices have hence been studied as combinations of TASEP segments with effective entrance and exit rates [21–23].

* Corresponding author.
E-mail address: adelaide.raguin@u-bordeaux.fr (A. Raguin).

https://doi.org/10.1016/j.physa.2026.131466
Received 12 November 2025; Received in revised form 12 February 2026
Available online 24 March 2026

Although no exact solution can be obtained in such complex cases, the mean-field approximation yields accurate predictions when compared to kinetic Monte Carlo simulations [22,24–26]. Structures with junctions are frequent in real-world systems, like road maps and eukaryote cytoskeleton. In the latter, the total length of filaments can exceed one metre while being confined in cells spanning a few tens of micrometres, resulting in very entangled and complex networks [27,28].

TASEP on branched lattices with either closed or open boundary conditions have already been investigated. For two loops that share a common site (the so-called "figure-of-eight"), with a bias at the junction, Embley et al. [24] showed a good agreement between mean-field analytical calculations and Monte Carlo simulations, which we later extended for any number of loops with complex kinetic rules at the junction site [26]. Following an analogous approach, Gupta et al. investigated bidirectional transport on a roundabout-like network with a finite particle reservoir [29]. In the case of open boundary conditions, that better reflect real systems in which particles can enter and leave the lattice, for instance, we modelled the cytoskeletal transport at the intersection of two microtubules. To do this, we first decomposed the trajectories of the molecular motors at the junction into branched and asymmetric lattices along which we investigated the transport properties [25]. On similar structures, with two segments upstream and one downstream of the junction (noted V(2:1)), the dynamics of the domain wall across the entire lattice has been characterised [30], and later extended to fourfold structures V(1:3), V(2:2), and V(3:1) [24]. Besides, a lattice with bidirectional segments connected through a bridging one has also been investigated [31]. Interconnecting higher (any) number of segments, Wang et al. analysed the TASEP dynamics at a Multiple-Input-Single-Output (MISO, V(m:1)) junction [32], and later at a Multiple-Input-Multiple-Output (MIMO, V(m:n)) junction [33]. TASEP dynamics on lattices with MIMO junctions have also been explored in other studies. For instance, Shao-Da et al. connected m upstream segments to n downstream ones (with $m < n$) as all-to-all, and considered a slowing down rate r when particles cross from upstream to downstream segments [34]. Other studies on MIMO junctions include the work of Midhat et al. that utilised a mean-field framework to show that the phases and their boundaries are strongly dependent not only on the number of upstream and downstream segments but also on the inter-particle interaction [35]. Later, they extended their framework to examine the transport dynamics on TASEP lattices with Langmuir kinetics (that includes particle creation and annihilation) [36], and with a finite number of particles [37].

Therefore, it appears that a comprehensive model of multiple upstream and downstream segments connected through a junction site where complex kinetic rules allow particles to pause, accelerate, or prefer a particular path is so far lacking. Yet, such a rich behaviour has been observed for the cytoskeletal transport of kinesin and dynein molecular motors along microtubules, that have for instance been shown to pause, pass, and switch tracks [27,38,39]. At a very distinct scale, pedestrian and motor vehicle traffic at road crossings also exhibits complex behaviour in terms of kinetics and trajectories.

To fill this gap, in this study, we focus on a MIMO junction, and specifically introduce generalised kinetic rules at the junction site, characterised by bias, absorption, and pumping rates. Given the complexity of such a lattice, we develop an original numerical method that includes constrained optimisation (CO), to solve the mean-field expression of the current–density relation, and thereby, determine the phase diagram of the lattice for varying parameter values. Additionally, we compare our results to stochastic simulations using the Gillespie algorithm with a random-sequential update. We set out by presenting the MIMO junction with complex kinetic rules and the formulation of current conservation in the mean-field, together with its numerical solution using a Phase Combination Matrix (PCM) and a CO solver. Then, we investigate in detail the transport phenomenology along the lattice. We observe that the properties of transport at the junction, typically depicted by the phase diagram, become highly complex and reflect the role of the bottleneck effect, itself dependent on the values of the structural and kinetic parameters at the junction.

2. The complex multiple-input-multiple-output (MIMO) junction

We focus on a multiple-input-multiple-output (MIMO) junction connecting any number of upstream and downstream segments, through an individual site, the junction (with density $\tilde{\rho}$ and current $\tilde{J}$), shared by all segments of the lattice (see Fig. 1). A reminder of previous TASEP results is provided in Appendix B. At the boundaries of the overall lattice, the upstream segments share a common

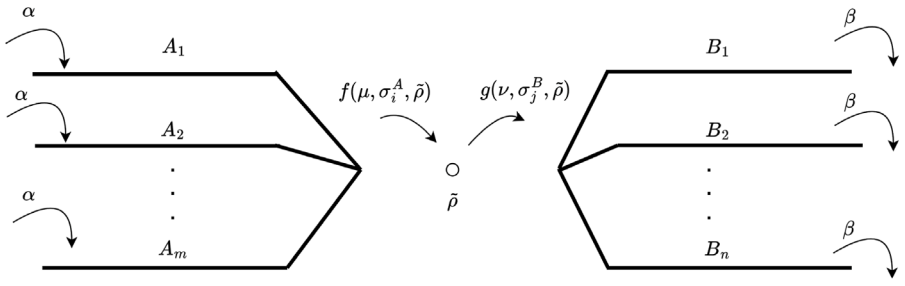

Fig. 1. TASEP on a lattice with a junction site connecting m upstream (noted A) and n downstream (noted B) segments, also called a multiple-input-multiple-output (MIMO) junction. α and β are the entrance and exit rates, at the left and right boundaries of the lattice, respectively. At the junction, the density is noted $\tilde{\rho}$, and each upstream segment A_i (with $i \in [1, \dots, m]$) and each downstream segment B_j (with $j \in [1, \dots, n]$) is associated with an individual bias value, noted σ_i^A and σ_j^B, respectively. Additionally, the rates for particles being absorbed into and pumped out of the junction, are noted as μ and ν, respectively. Within the bulk of each of the segments, the jumping rate γ is equal to 1.

entrance rate α and the downstream segments share a common exit rate β. Conversely, at segment ends connected to the junction site, each upstream segment (noted A_i with $i \in [1, \dots, m]$) is characterised by an individual effective exit rate (noted β_{eff_i}) that depends on the junction density ($\tilde{\rho}$), the specific bias (σ_i^A) for that segment, and the rate for absorbing particles into the junction (noted μ). Analogously, each downstream segment (noted B_j with $j \in [1, \dots, n]$) is characterised by an individual effective entrance rate (noted α_{eff_j}) that depends on the junction density ($\tilde{\rho}$), the specific bias (σ_j^B) for that segment, and the rate for pumping particles out of the junction (noted ν). The biases for the upstream and downstream segments each sum up to 1, *i.e.*

$$\sum_i (\sigma_i^A) = \sum_j (\sigma_j^B) = 1. \tag{1}$$

Increasing the bias on an upstream segment (σ_i^A) increases the probability that particles exit that segment to the junction. Likewise, increasing the bias on a downstream segment (σ_j^B) increases the probability that particles leaving the junction enter that segment. Opposite effects are implied when instead decreasing the biases. Thus, the bias creates an asymmetry amongst segments, while the topology of the whole lattice remains unchanged.

Since we consider that throughout the bulk of the segments, the jumping rate γ is equal to 1, the transport properties of the lattice are controlled by the boundary rates of the individual segments. Based on the well-established results for a single TASEP segment (see Table B.3 in Appendix B), we introduce the Phase Combination Matrix (PCM) to define a unique combination of phases on the distinct individual segments of the overall lattice, in a way that can easily be interpreted numerically. As illustrated in Fig. 2, the PCM takes the form of a binary matrix with dimensions $4 \times (m + n)$. Each row corresponds to a phase in the following order: high density (HD), low density (LD), maximal current (MC), and shock phase (SP). The m leftmost columns correspond to the A segments, while the n rightmost columns correspond to the B segments. For example, if PCM[3][m+2] = 1, then the segment B_2 is in the maximal current phase. Since a segment can be in only one single phase depending on its boundary conditions, all the elements in each column sum up to 1.

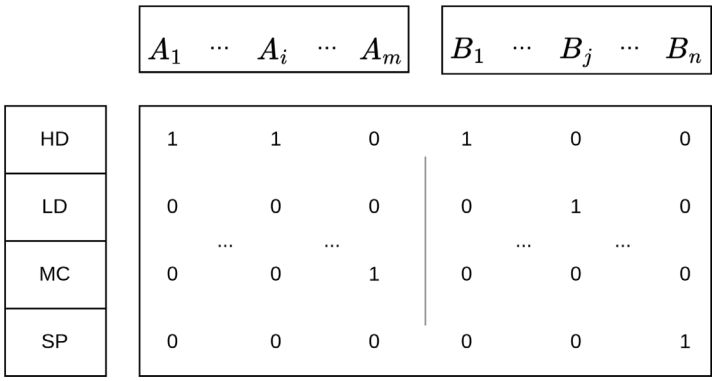

Fig. 2. The Phase Combination Matrix (PCM) is a binary matrix of dimension $4 \times (m + n)$ which defines a unique combination of phases along the lattice. Each row represents a phase and each column a segment.

3. Mean-field expression of current conservation at the complex MIMO junction

Our numerical approach to compute the phase diagram is based on the mean-field theory and the effective entrance and exit rates of the segments. Detailed calculation steps have been explained in our previous study for threefold lattices [25]. The effective exit rate of the ith upstream segment (β_{eff_i}) can be expressed as the product of the absorption rate at the junction (μ), the bias of the ith upstream segment (σ_i^A), and the density of holes at the junction ($1 - \tilde{\rho}$):

$$\beta_{eff_i} = \mu \sigma_i^A (1 - \tilde{\rho}). \tag{2}$$

Analogously, the effective entrance rate of the jth downstream segment (α_{eff_j}) can be expressed as the product of the pumping rate (ν), the bias of the jth downstream segment (σ_j^B), and the density of particles at the junction ($\tilde{\rho}$):

$$\alpha_{eff_j} = \nu \sigma_j^B \tilde{\rho}. \tag{3}$$

Then, a necessary condition for a phase combination to arise along the lattice is to fulfil the current conservation at the junction. It allows determining the physically feasible value(s) for $\tilde{\rho}$ such that the phase combination arises:

$$\sum_{i=1}^{m} J_{A_i} = \sum_{j=1}^{n} J_{B_j}, \tag{4}$$

where J_{A_i} is the current on the segment A_i and J_{B_j} the one on the segment B_j. Hence, the expressions for J_{A_i} and J_{B_j} have at most one unknown variable $\tilde{\rho}$, with a maximum degree of two. Thus, Eq. (4) can be simplified as a polynomial of at most degree two:

$$a\tilde{\rho}^2 + b\tilde{\rho} + c = 0, \tag{5}$$

Table 1
Expressions for the coefficients of Eq. (5) of current conservation at the junction.

Density	A Segments			B Segments		
Phase	a_{A_i}	b_{A_i}	c_{A_i}	a_{B_j}	b_{B_j}	c_{B_j}
HD	$-(\mu\,\sigma_i^A)^2$	$2\,(\mu\,\sigma_i^A)^2 - \mu\,\sigma_i^A$	$\mu\,\sigma_i^A - (\mu\,\sigma_i^A)^2$	0	0	$\beta\,(1-\beta)$
LD	0	0	$\alpha\,(1-\alpha)$	$-(\nu\,\sigma_j^B)^2$	$\nu\,\sigma_j^B$	0
MC	0	0	$\frac{1}{4}$	0	0	$\frac{1}{4}$
SP	0 $-(\mu\,\sigma_i^A)^2$	0 $2(\mu\,\sigma_i^A)^2 - \mu\,\sigma_i^A$	$\alpha\,(1-\alpha)$ $\mu\,\sigma_i^A - (\mu\,\sigma_i^A)^2$	0 $-(\nu\,\sigma_j^B)^2$	0 $\nu\,\sigma_j^B$	$\beta\,(1-\beta)$ 0

where, $a = \sum_i a_{A_i} - \sum_j a_{B_j}$, $b = \sum_i b_{A_i} - \sum_j b_{B_j}$, and $c = \sum_i c_{A_i} - \sum_j c_{B_j}$. The expressions for the coefficients of the quadratic Eq. (5) are summarised in Table 1. The detailed calculation steps can be found in Appendix C.

From Eq. (5), we determine the value of $\tilde{\rho}$, and deduce the effective exit rates β_{eff_i} and the effective entrance rates α_{eff_j} of the upstream and downstream segments, respectively (using Eqs. (2) and (3), respectively). Knowing the conditions on the boundary rates of an individual segment for a phase to arise (see Table B.3), a second necessary condition for a phase combination to arise along the overall lattice is that the boundary rates of each segment fulfil the conditions summarised in Table 2. Eventually, certain combinations of phases cannot arise due to contradictory conditions on α and β, *i.e.*:

- $\forall\, i,k$ with $i,k \in [1,\dots,m]$ and $i \neq k$, if A_i is in the MC phase, A_k cannot be in LD or SP because of contradictory constraints on α
- $\forall\, j,l$ with $j,l \in [1,\dots,n]$ and $j \neq l$, if B_j is in the MC phase, B_l cannot be in HD or SP because of contradictory constraints on β

Table 2
Conditions on the boundary rates for the different phases.

Phase	A Segments	B Segments
HD	$\mu\,\sigma_i^A\,(1-\tilde{\rho}) < \frac{1}{2}$ $\mu\,\sigma_i^A\,(1-\tilde{\rho}) < \alpha$	$\beta < \frac{1}{2}$ $\beta < \nu\,\sigma_j^B\,\tilde{\rho}$
LD	$\alpha < \frac{1}{2}$ $\alpha < \mu\,\sigma_i^A\,(1-\tilde{\rho})$	$\nu\,\sigma_j^B\,\tilde{\rho} < \frac{1}{2}$ $\nu\,\sigma_j^B\,\tilde{\rho} < \beta$
MC	$\alpha > \frac{1}{2}$ $\mu\,\sigma_i^A\,(1-\tilde{\rho}) > \frac{1}{2}$	$\beta > \frac{1}{2}$ $\nu\,\sigma_j^B\,\tilde{\rho} > \frac{1}{2}$
SP	$\alpha < \frac{1}{2}$ $\alpha = \mu\,\sigma_i^A\,(1-\tilde{\rho})$	$\beta < \frac{1}{2}$ $\beta = \nu\,\sigma_j^B\,\tilde{\rho}$

4. Numerical approach

4.1. Numerical solutions of the mean-field current conservation equations

In the MIMO TASEP junction with complex kinetic rules, the number of possible phase combinations may blow up exponentially. For instance, along a V(2:3) lattice, the number of possible phase combinations becomes $4^{2+3} = 1024$. To tackle this challenge for a MIMO junction with complex kinetic rules, we develop a generic numerical approach, coded in Python. The algorithm takes as input the number of upstream and downstream segments (m and n, respectively), the absorption and pumping rates (μ and ν, respectively), and the upstream and downstream biases (σ_i^A and σ_j^B, respectively). It provides as output: (i) the phase diagram; (ii) the densities at the junction and on the individual upstream and downstream segments ($\tilde{\rho}$, ρ_{A_i}, and ρ_{B_j}, respectively); and (iii) the currents at the junction and along the individual upstream and downstream segments ($\tilde{J}$, J_{A_i}, and J_{B_j}, respectively), for each (α,β) pair.

The algorithm starts by generating a PCM for each potential phase combination, and checking the constraints on α and β which do not depend on $\tilde{\rho}$. Next, the current conservation (Eq. (5)) is solved to obtain the value of $\tilde{\rho}$. However, when $a,b,c = 0$, Eq. (5) returns no information. To mitigate this, we made use of a Constrained Optimisation (CO) approach [40]. The CO solver tries to find a value for $\tilde{\rho}$ which satisfies all the constraints on both the entrance and exit rates of all segments, after we defined the problem as follows:

$$
\begin{aligned}
&\text{minimise} && \tilde{\rho} \\
&\text{subject to.} && g(\tilde{\rho}) = 0 \quad \text{with } g : \mathbb{R} \to \mathbb{R}^p \text{ for p equality constraints} \\
&&& h(\tilde{\rho}) \geq 0 \quad \text{with } h : \mathbb{R} \to \mathbb{R}^q \text{ for q inequality constraints}
\end{aligned}
$$

Both the equality and inequality constraints are listed in Table 2, and depend on the respective phase of each segment. We use the Python package "scipy.optimize" and opt for the "minimize" function using the "COBYLA" method which consists in solving

the constrained optimisation by linear approximation. For each set of constraints, we verified that only one solution exists for $\tilde{\rho}$ since both the "maximize" and "minimize" functions of the "scipy.optimize" package return the same $\tilde{\rho}$ value.

Finally, we obtain the value of $\tilde{\rho}$ (by solving Eq. (5) or from the CO solver) and substitute it in the constraints listed in Table 2. If all conditions are fulfilled, we affirm that the phase combination occurs for the given (α, β) pair.

4.2. Stochastic simulations

Stochastic simulations of the transport along the overall lattice are performed in C++, following a Gillespie algorithm [41,42], with each segment having a length $L = 100$ sites. We define a $cycle$ as a time-unit, whose duration depends on the lattice size as: $cycle = L(m+n)$, such that, during a cycle, all particles along the overall lattice are picked once on average. We record the dynamics (densities and currents at the junction and along each segment) after each cycle, only in the steady state (*i.e.* after 10^4 cycles).

5. Model phenomenology

We define a notation for a combination of phases, as illustrated with the following example: $X.Y : nZ$ denotes a phase combination for a V(2:n) vertex with upstream segments in phases X and Y, while all n downstream segments are in the phase Z. X, Y, and Z can be LD, HD, MC, or SP.

5.1. MIMO junction with neutral bias and without bottleneck effect

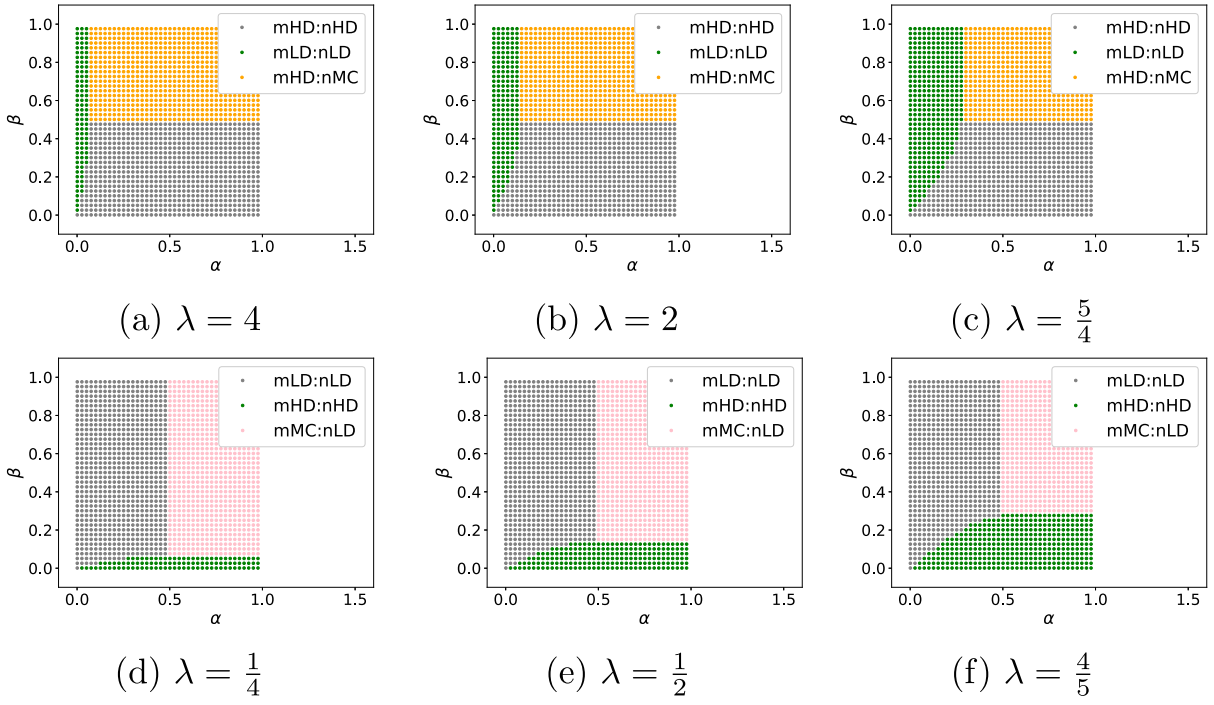

Fig. 3. Phase diagrams of V(m:n) lattices obtained by numerically solving the mean-field current conservation at the junction, for $\lambda > 1$: (a) V(4:1), (b) V(4:2), and (c) V(5:4); and $\lambda < 1$: (d) V(1:4), (e) V(2:4), and (f) V(4:5); with neutral bias and without bottleneck effect.

We define the ratio λ as:

$$\lambda = \frac{m}{n}. \tag{6}$$

Fig. 3 shows the phase diagrams of the V(m: n) lattices for $\lambda > 1$ and $\lambda < 1$ obtained from the numerical approach described in Section 4.1, with neutral bias (*i.e.* $\forall i \in [1, \dots, m], \sigma_i^A = \frac{1}{m}$ and $\forall j \in [1, \dots, n], \sigma_j^B = \frac{1}{n}$) and absorption and pumping rates sufficiently high to avoid bottleneck effect (the conditions for the bottleneck effect to arise are presented in the paragraph 5.2.1). We observe that lattices with the same λ value have the same phase diagram, as previously did Liu and Wang [33]. Both Figs. 3(a), (b), and (c), and Figs. 3(d), (e), and (f) have 3 distinct phases, including mLD:nLD (grey) and mHD:nHD (green). However, while (a), (b), and (c) ($\lambda > 1$) show a mHD:nMC phase (yellow); (d), (e), and (f) ($\lambda < 1$) show a mMC:nLD phase (pink). In either case, since the MC phase occurs on the side of the junction with the lower number of segments, owing to the conservation of current, each segment

on the opposite side has a current value of $J = \frac{1}{4}\frac{\min(m,n)}{\max(m,n)}$. When considering the cases $\lambda_1 = \frac{1}{\lambda_2}$, *i.e.* (a) *versus* (d), (b) *versus* (e), and (c) *versus* (f), we observe that the surfaces occupied by the mLD:nLD and mHD:nHD phases, respectively, are symmetric with respect to the $\alpha = \beta$ line of the phase diagram. In other words, if we invert the entrance and exit rates of the overall lattice (α and β, respectively) and that we also invert the number of upstream and downstream segments, owing to the particle–hole symmetry that ensures that moving particles to the right is equivalent to moving holes to the left (explained in further detail in [26]), we recover the same diagram.

From Figs. 3(a), (b), and (c), it can be observed that increasing the value of λ moves the phase boundary separating mLD:nLD (in grey) from mHD:nHD (in green), and mHD:nMC (in yellow) closer to the y-axis ($\alpha = 0$), decreasing the area under the mLD:nLD phase. For a fixed number of downstream segments, increasing the number of upstream segments (and thereby λ) saturates the junction, making it harder for particles to exit the lattice. Thus, for a given β, the entrance rate α must be lower for the whole system to be in the LD phase (mLD:nLD). Analogous observations can be made from Figs. 3(d), (e), and (f), with regards to the mHD:nHD phase, which moves closer to the x-axis ($\beta = 0$) as λ decreases, *i.e.* the number of downstream segments increases with respect to the number of upstream ones, making it easier for particles to exit the lattice. For symmetric lattices ($\lambda = 1$) without bottleneck effect, the phase diagram remains the same as that of a simple TASEP segment (see Fig. B.12(b)).

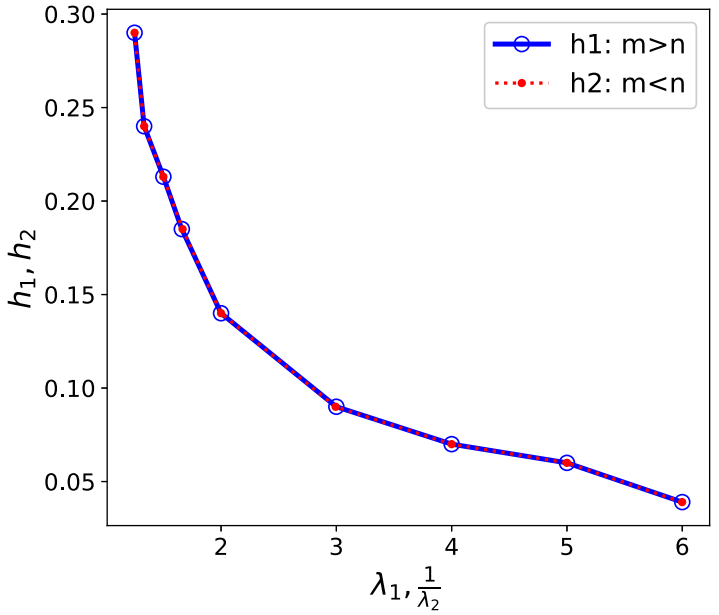

Fig. 4. Plots of h_1 *vs* λ_1, and h_2 *vs* $\frac{1}{\lambda_2}$ overlap when $\lambda_1\lambda_2 = 1$. Results are obtained *via* numerical analysis of lattices V(a:b) with $\lambda_1 > 1$ and V(b:a) with $\lambda_2 < 1$ with $((a, b) \in [(2, 1), (3, 1), (4, 1)(5, 1), (6, 1)])$.

In Fig. 4, we plot the distance (h_1) between the y-axis and the boundary delimiting the mLD:nLD phase from the mHD:nMC one *versus* λ_1 ($\lambda_1 > 1$), overlaid with the distance (h_2) between the x-axis and the boundary delimiting the mHD:nHD phase from the mMC:nLD one *versus* $\frac{1}{\lambda_2}$ ($\lambda_2 < 1$). The complete overlap of the points confirms the particle–hole symmetry.

5.2. MIMO junction with neutral bias and with bottleneck effect

5.2.1. Conditions for the bottleneck effect

We define the bottleneck effect in a V(m: n) lattice as the scenario when the current is impeded by low absorption (μ) and/or pumping (ν) rates at the junction site (and/or the bias, if present), such that the Maximal Current (MC) phase cannot arise simultaneously on all segments on the side of the junction with the lower number of segments. On the side with higher number of segments, owing to current conservation at the junction, all segments cannot be in MC phase simultaneously, independent of the parameter values at the junction. We introduce the parameter θ, called the bottleneck coefficient, to quantify the reduction of current due to the bottleneck effect. θ is defined (in percentage) as the maximal current achieved by the lattice (j_{max}) divided by the maximal current achievable in the absence of bottleneck effect:

$$\theta = \frac{j_{max}}{J_{MC}.\ \min(m,n)} \times 100 = \frac{j_{max}}{\frac{1}{4}.\ \min(m,n)} \times 100. \tag{7}$$

We define as ψ the lowest value that ensures $\theta = 100\%$, when $\mu = \nu = \psi$. The bottleneck effect arises if either one of the three following conditions is satisfied: $\mu, \nu < \psi$ or $\mu \leq \mu^*$ or $\nu \leq \nu^*$. Here, μ^* and ν^* are lower thresholds of the absorption and pumping

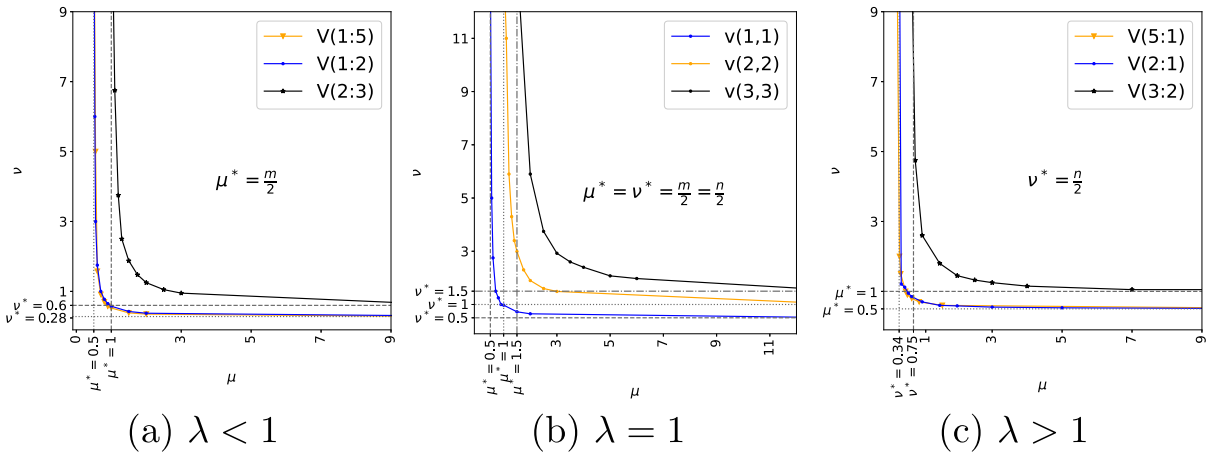

Fig. 5. Diagrams delimiting the areas with and without bottleneck effect, depending on the values of the absorption (μ) and pumping (ν) rates, obtained from the numerical solutions of the mean-field equations: (a) $\lambda < 1$ *e.g.* V(1:2), V(1:5) and V(2:3); (b) $\lambda = 1$ *e.g.* V(1:1), V(2:2) and V(3:3); and (c) $\lambda > 1$ *e.g.* V(3:2), V(2:1) and V(5:1). For each lattice, the area below the curve represents (μ, ν) pairs that result in the bottleneck effect, unlike above the curve. The dotted lines show the lower threshold values of the absorption (μ^*) and pumping (ν^*) rates.

rates, respectively, below which the bottleneck effect appears, irrespective of the values of the other parameters. The bottleneck effect also arises for $\mu^* < \mu < \psi$ and $\nu > \psi$ in case ν is not high enough to compensate for the low absorption rate (μ) (and *vice versa*). Fig. 5 shows the (μ, ν) pairs resulting in a bottleneck effect for lattices with $\lambda < 1$, $\lambda = 1$, and $\lambda > 1$. In each diagram, the curve separating the areas with (below the curve) and without (above the curve) bottleneck effect asymptotically converges towards the thresholds μ^* and ν^* along the x- and y-axis, respectively.

The expression of ψ depends on m, n, and $\tilde{\rho}$ as follows (detailed calculation steps are provided in Appendix D):

- if $\lambda = 1$,

$$\psi = m = n, \tag{8}$$

- if $\lambda < 1$,

$$\psi = \frac{n}{2\tilde{\rho}}\left(1 - \sqrt{1 - \frac{m}{n}}\right), \tag{9}$$

- if $\lambda > 1$,

$$\psi = \frac{m}{2(1-\tilde{\rho})}\left(1 - \sqrt{1 - \frac{n}{m}}\right). \tag{10}$$

It is worth noting that the value of ψ will be the same for both V(a:b) and V(b:a) $\forall\, a, b \in \mathbb{N}$. Without loss of generality, we can assume that $a < b$, with $\tilde{\rho}_1$ being the density at the junction for V(a:b) and $\tilde{\rho}_2$ the one for V(b:a). Then, the values of ψ_1 and ψ_2 can be expressed as, $\psi_1 = \frac{b}{2\tilde{\rho}_1}\left(1 - \sqrt{1 - \frac{a}{b}}\right)$ and $\psi_2 = \frac{b}{2(1-\tilde{\rho}_2)}\left(1 - \sqrt{1 - \frac{a}{b}}\right)$, respectively. From particle–hole symmetry, we know that the density of particles in V(a:b) equals the density of holes in V(b:a), *i.e.* $\tilde{\rho}_1 = 1 - \tilde{\rho}_2$; and thus $\psi_1 = \psi_2$. Eqs. (8), (9), and (10) can be expressed in the generalised form as:

$$\psi = \frac{\max(m,n)}{2 \times \min(\tilde{\rho}, (1-\tilde{\rho}))}\left(1 - \sqrt{1 - \frac{\min(m,n)}{\max(m,n)}}\right). \tag{11}$$

5.2.2. Current–density relation at the junction when $\lambda = 1$

Fig. 6 shows the impact of the bottleneck effect on the current–density relation at the junction of a V(1:1) lattice. For the three cases considered, the stochastic simulation results and the numerical solutions of the mean-field expressions are in good agreement. In panel (a), when the bottleneck effect is caused by a low absorption rate ($\mu < \nu$), the density at the junction ($\tilde{\rho}_{\bar{j}_{max}}$) at which the maximal value of current is observed is lower than 0.5, and it shifts further left with increasing $|\mu - \nu|$. In panel (b), when the bottleneck effect is caused by equally low absorption and pumping rates, the maximal value of current is still observed at the density $\tilde{\rho}_{\bar{j}_{max}} = 0.5$. In panel (c), when the bottleneck effect is caused by a low pumping rate ($\mu > \nu$), the density $\tilde{\rho}_{\bar{j}_{max}}$ at which the maximal value of current is observed is higher than 0.5, and it shifts further right with increasing $|\mu - \nu|$. In all three cases, as at least one of the rates decreases (μ in (a), μ and ν in (b), and ν in (c)), the maximal value of the current decreases, which corresponds to a stronger bottleneck effect.

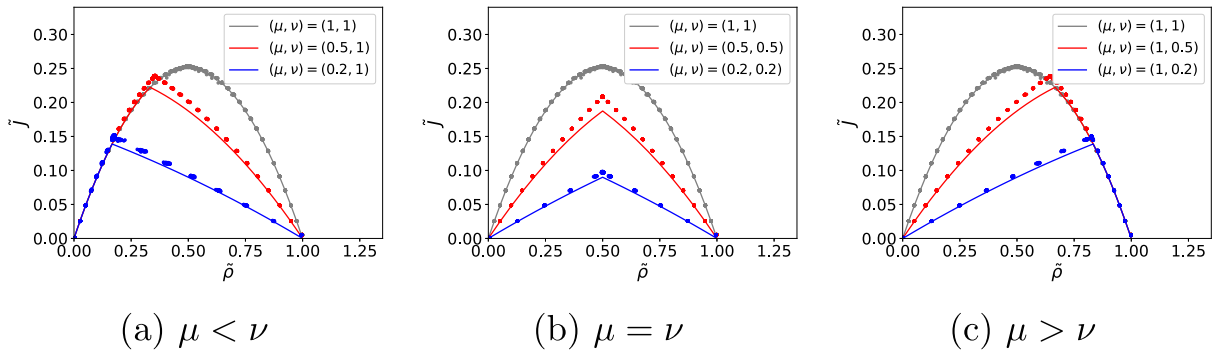

Fig. 6. Current–density relation at the junction of a V(1:1) lattice (with $L = 100$ sites) for varying μ and ν values. (a) $\mu < \nu$, the curve becomes asymmetric and the maximum current is observed for $\tilde{\rho} < 0.5$. (b) $\mu = \nu$, the curve remains symmetric along $\tilde{\rho} = 0.5$, but is lower for lower values of μ and ν. (c) $\mu > \nu$, the curve becomes asymmetric and the maximum current is observed for $\tilde{\rho} > 0.5$. The points correspond to stochastic simulation results based on the Gillespie algorithm, and the lines to the numerical solutions of the mean-field equations.

In panel (a), for a low density at the junction ($\tilde{\rho}$) the current–density relation is similar to that of the case without bottleneck effect (grey curve $\mu = \nu = 1$). However, when $\tilde{\rho}$ reaches a certain value ($\tilde{\rho}_{\tilde{J}_{max}} < 0.5$), the density at the upstream site before the junction saturates, and particles are pumped out of the junction as soon as they enter it ($\mu < \nu$), such that the density on the site after the junction rapidly increases. Interestingly, the current–density relation at the junction in this regime is not anymore quadratic but quasi-linear, suggesting that the current to move particles into the junction becomes only dependent on the density of holes at the junction. In panel (c), for a low density at the junction ($\tilde{\rho}$), the current–density relation is not anymore quadratic but quasi-linear, suggesting that the density on the site just after the junction, which depends on $\nu < \mu$, is low enough such that the current to move particles out of the junction becomes only dependent on the density of particles at the junction. As the density at the junction reaches a certain value ($\tilde{\rho}_{\tilde{J}_{max}} > 0.5$), the site just after the junction becomes populated, implying that the current–density relation recovers a quadratic form, similar to that of the case without bottleneck effect (grey curve $\mu = \nu = 1$). While in panel (a) the current reaches its maximal value for a density below 0.5 because the junction tends to be emptied as soon as it is filled ($\mu < \nu$), in panel (c) this value is above 0.5 because the junction tends to be filled as soon as it is emptied ($\mu > \nu$). In panel (b) the effects observed in panels (a) and (c) are combined such that for $\tilde{\rho} < 0.5$ the impact of the reduced pumping rate dominates and the current–density relation seems to depend only on the density of particles at the junction, and for $\tilde{\rho} > 0.5$ the impact of the reduced absorption rate dominates and the current–density relation seems to depend only on the density of holes at the junction.

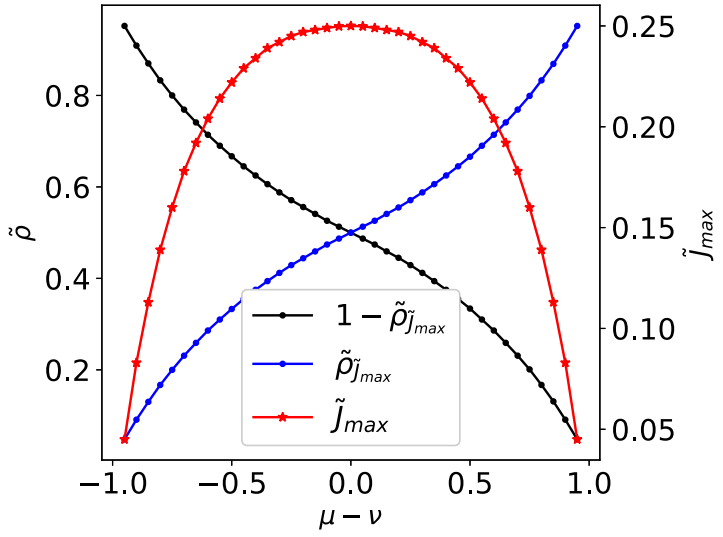

Fig. 7. Maximal value of the current at the junction ($\tilde{J}_{max}$) and corresponding density (of particles, $\tilde{\rho}_{\tilde{J}_{max}}$ and holes, $1 - \tilde{\rho}_{\tilde{J}_{max}}$) *versus* $\mu - \nu$, for a V(1:1) lattice when $\max(\mu, \nu) = \psi_{V(1:1)} = 1$ (see Eq. (8)). Results are obtained by numerically solving the mean-field equations.

Fig. 7 illustrates how the maximal value of the junction current ($\tilde{J}_{max}$, in red) and its corresponding junction density of particles ($\tilde{\rho}_{\tilde{J}_{max}}$, in blue) and holes ($1 - \tilde{\rho}_{\tilde{J}_{max}}$, in black) are affected by the difference between the absorption and pumping rates ($\mu - \nu$),

with $\max(\mu, \nu) = \psi_{V(1:1)} = 1$ (see Eq. (8)). As $\mu - \nu$ increases, the current $\tilde{J}_{max}$ follows an inverted parabola profile depending on the density $\tilde{\rho}_{\tilde{J}_{max}}$, whereas $\tilde{\rho}_{\tilde{J}_{max}}$ increases in a non-linear monotonic fashion depending on $\mu - \nu$. As a result, the profile of $\tilde{J}_{max}$ depending on $\mu - \nu$ shown in Fig. 7 deviates from an inverted parabola, with a stronger effect for the intermediate values of $\mu - \nu$. On the left, $\mu = 0$ and $\nu = 1$, particles cannot enter the junction but could possibly leave it, and so both the particle density and the current at the junction are null. In the centre, $\mu = \nu = 1$, $\tilde{\rho}_{\tilde{J}_{max}} = 0.5$, and the maximal current at the junction is equal to that of the Maximal Current phase ($\tilde{J}_{max} = J_{MC} = \frac{1}{4}$). On the right, $\mu = 1$ and $\nu = 0$, particles can enter the junction but cannot leave it, and so the particle density $\tilde{\rho}_{\tilde{J}_{max}} = 1$ but the current $\tilde{J}_{max} = 0$. When considering the symmetry along the line $\mu - \nu = 0$, it is apparent that exchanging μ and ν, the current at the junction ($\tilde{J}_{max}$) remains unchanged while the density of particles ($\tilde{\rho}_{\tilde{J}_{max}}$) is now equal to that of the holes ($1 - \tilde{\rho}_{\tilde{J}_{max}}$). Together, these features are consequences of the particle–hole symmetry at the junction.

5.2.3. Current at the junction when λ varies

Fig. 8 shows the effect of the number of upstream (m) and downstream (n) segments on the bottleneck coefficient (θ) for fixed absorption and pumping rates ($\mu = \nu = 1$). When either or both of m and n equals 1, the maximal value of current at the junction is equal to that of the Maximal Current phase on the side of the junction with the lower number of segments, such that $\tilde{J}_{max} = J_{MC} \cdot \min(m, n) = \frac{1}{4} \cdot \min(m, n)$, meaning that the absorption and/or pumping rates are high enough so that no bottleneck effect is observed. When either or both of m and n increases, the absorption and/or pumping rates are not high enough to avoid the bottleneck effect, and consequently θ decreases. While for a fixed number of upstream segments (m) increasing the number of downstream segments (n) till $n = m$ leads to a decrease of θ, increasing n even further increases θ very slightly. A similar behaviour is observed when instead n is kept fixed and m is increased. The slight increase in the θ value upon increasing either m or n beyond the symmetric configuration, can be attributed to the fact that $\psi(V(a{:}\ a)) > \psi(V(a{:}\ b))\ \forall b \neq a$ (see Eqs. (8)–(11)). In other words, when moving away from the diagonal $m = n$ in Fig. 8, ψ decreases, which leads to a reduction in the bottleneck effect and an increase in the bottleneck coefficient (θ), for fixed μ and ν values less than ψ.

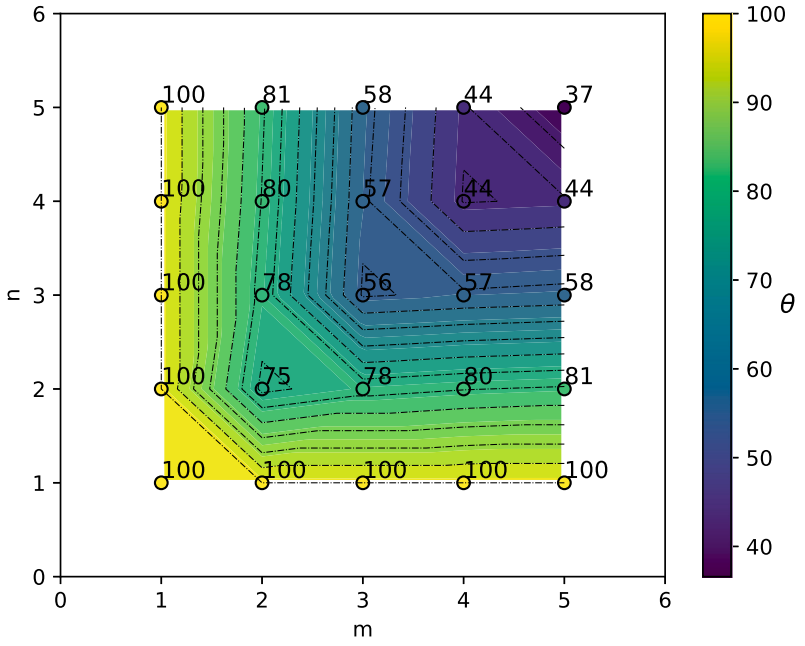

Fig. 8. Impact of the number of upstream (m) and downstream (n) segments on the bottleneck coefficient (θ) for fixed absorption and pumping rates ($\mu = \nu = 1$). θ is symmetric across the diagonal ($m = n$) and equals 100% if either or both of m and n are equal to 1.

5.3. MIMO junction with bias

5.3.1. Methodological limitations

As explained in Section 4.1, phase diagrams are obtained from the numerical solutions of the mean-field equations, using values of α and β on a grid. Because the Shock Phases occur along lines or even points (and not surfaces) and it is not possible to cover all the real values between 0 and 1 for α and β, it is not always possible to capture the Shock Phases. Consequently, we acknowledge that the phase diagrams (Figs. 9, 10, and F.14) do not cover all the Shock Phases of the system, yet, it is valid that each segment transits between LD and HD phases *via* either a Shock Phase or a Maximal Current phase.

5.3.2. Lattices with $\lambda = 1$

Fig. 9 shows the phase diagrams for a V(2:2) lattice, with different bias configurations. Panel (a), with neutral bias, is similar to that of a simple TASEP segment (see Fig. B.12) with particle–hole symmetry along the $\alpha = \beta$ line, and equal areas for the 2HD:2HD and the 2LD:2LD phases, while the Shock Phase lies along the line $\alpha = \beta < 0.5$ and the top-right area is occupied by the 2MC:2MC phase. Precisely, for this neutral bias lattice, the Shock Phase consists in a Domain Wall that can be equally likely located on any segment of the lattice where it randomly fluctuates.

Panel (b), with biases on the upstream segments ($\sigma^A = [0.25, 0.75]$), shows that the region previously occupied by the 2MC:2MC phase is now by a HD.MC:2LD phase, because particles on the upstream segment with reduced bias ($\sigma_i^A = 0.25$) can less easily exit into the junction, turning the segment from MC to HD. As the current entering the junction reduces, the density downstream the junction, on B segments, reduces too, which causes them to have a LD phase. For the same reason, when α increases or β decreases, the upstream segment with low bias ($\sigma_i^A = 0.25$) turns into HD, while the one with high bias ($\sigma_i^A = 0.75$) may still sustain LD or change to MC. Thus, besides 2HD:2HD, 2LD:2LD, and HD.MC:2LD, three new phases appear, namely HD.LD:2HD, HD.MC:2HD, and HD.LD:2LD. One can note that while the upstream segment with a low bias gets filled through a Shock Phase, the favoured one reaches a MC phase.

Panel (c), with biases on the downstream segments ($\sigma^B = [0.25, 0.75]$), can be obtained from panel (a), by particle–hole symmetry, exchanging upstream and downstream segments, α and β, and LD and HD phases. In this case, the reduced bias on one B segment limits particle entry from the junction, which in turn increases the density on upstream segments.

Panel (d), with equally biased upstream and downstream segments ($\sigma^A = \sigma^B = [0.25, 0.75]$), shows that, similar to panel (a), the phase diagram is symmetric along the line $\alpha = \beta$, which is again a consequence of the particle–hole symmetry. When compared with panel (a), panel (d) shows that the 2MC:2MC phase becomes a HD.MC:LD.MC, because MC occurs only on the highly biased

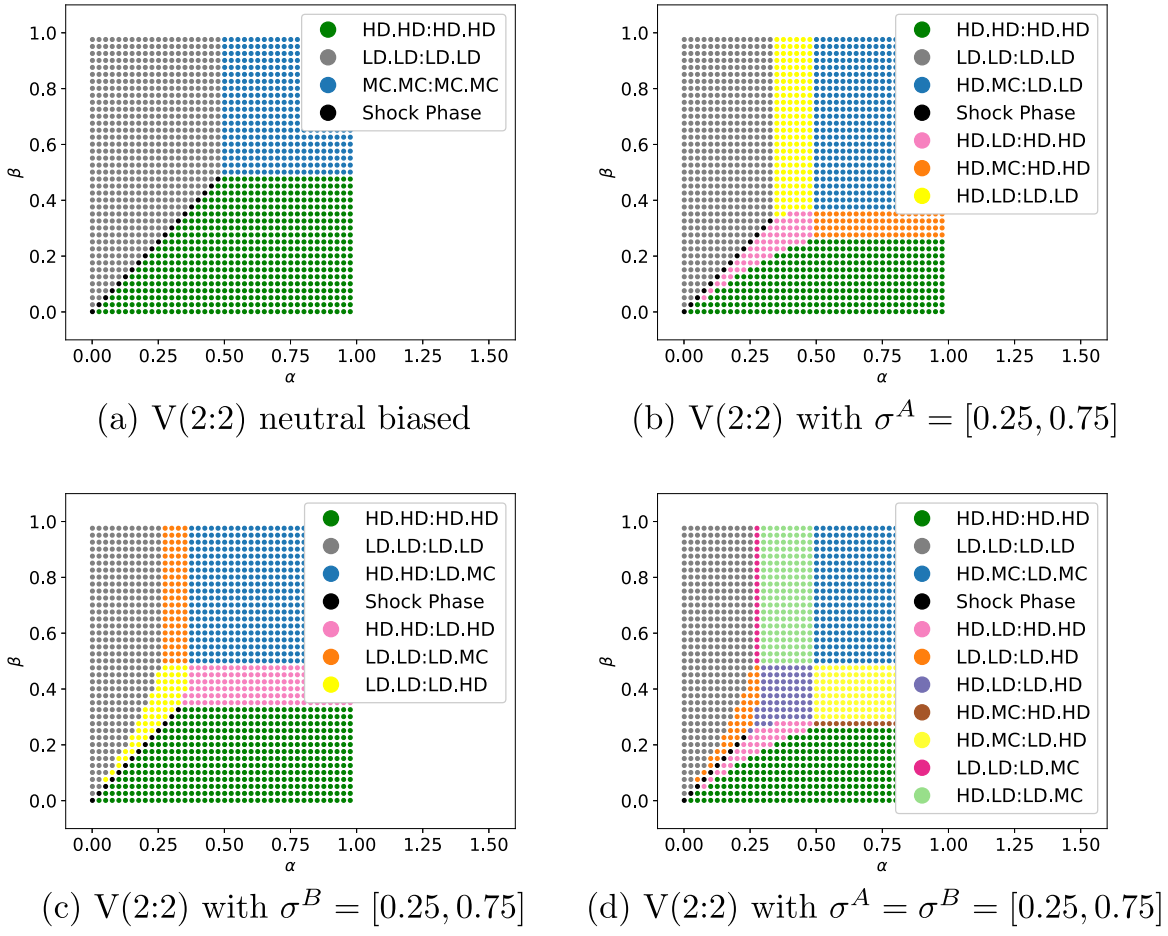

(a) V(2:2) neutral biased (b) V(2:2) with $\sigma^A = [0.25, 0.75]$

(c) V(2:2) with $\sigma^B = [0.25, 0.75]$ (d) V(2:2) with $\sigma^A = \sigma^B = [0.25, 0.75]$

Fig. 9. Phase diagrams obtained from the numerical solutions of the mean-field equations for a V(2:2) lattice with: (a) neutral bias, (b) bias on only upstream segments, $\sigma^A = [0.25, 0.75]$, (c) bias on only downstream segments, $\sigma^B = [0.25, 0.75]$, and (d) equal biases on both upstream and downstream segments, $\sigma^A = \sigma^B = [0.25, 0.75]$. When both the upstream and downstream segments have the same biases, HD and LD phases across the individual segments are symmetric along the $\alpha = \beta$ diagonal.

segments. Whether α increases or β decreases, the downstream segments undergo a phase transition before the upstream ones, despite the bottleneck effect at the junction. Precisely, particles accumulate in the system first on the downstream segments, and then on the upstream ones, thereby filling the lattice in the direction opposite the particle flow.

5.3.3. Lattices with $\lambda > 1$

Fig. 10 shows the phase diagrams for a V(3:2) lattice, with different bias configurations. Panel (a), with neutral bias, is similar to Figs. 3(a–c), showing the phases 3HD:2HD, 3HD:2MC, and 3LD:2LD. In particular, 3HD:2HD and 3LD:2LD are present in all Fig. 10 cases, irrespective of the choice of biases across the upstream and/or downstream segments.

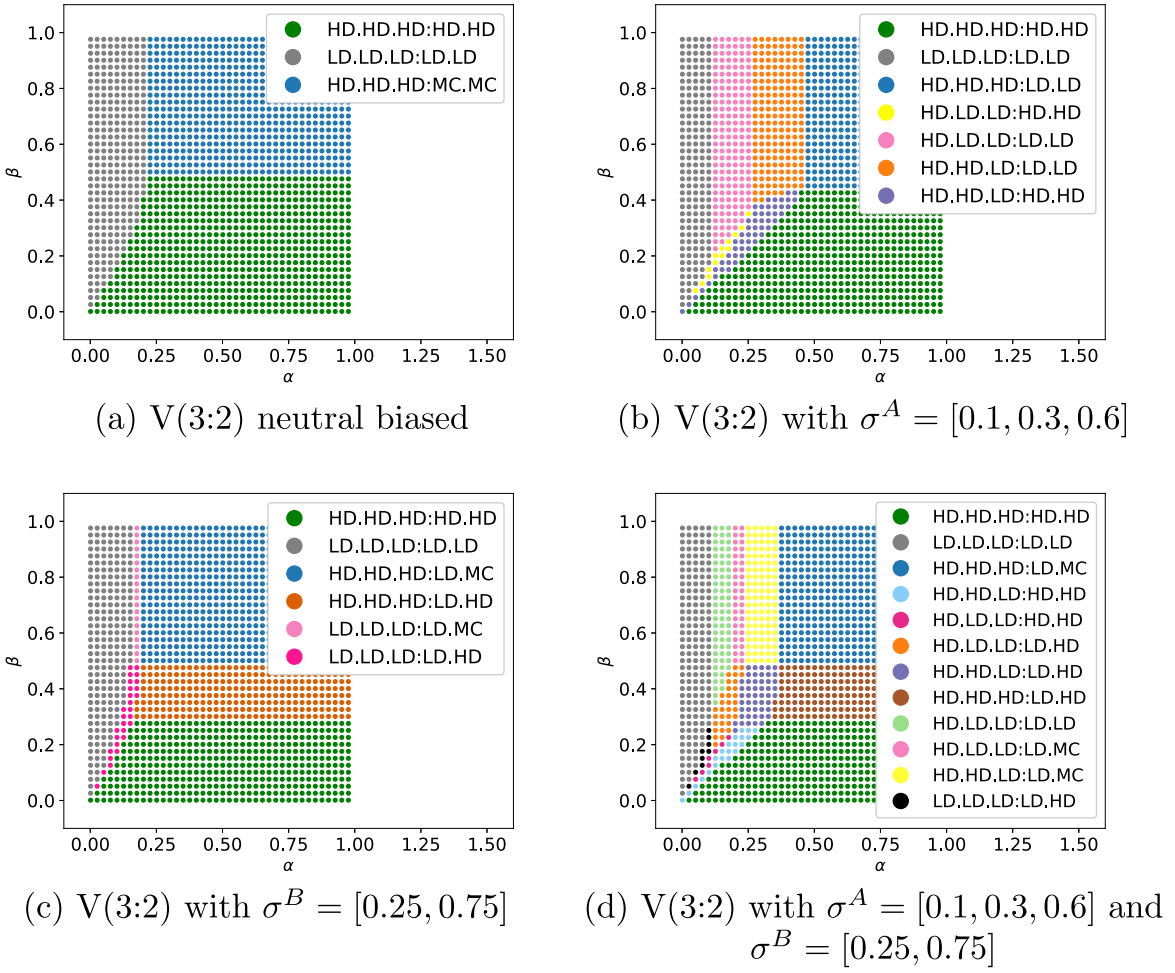

(a) V(3:2) neutral biased

(b) V(3:2) with $\sigma^A = [0.1, 0.3, 0.6]$

(c) V(3:2) with $\sigma^B = [0.25, 0.75]$

(d) V(3:2) with $\sigma^A = [0.1, 0.3, 0.6]$ and $\sigma^B = [0.25, 0.75]$

Fig. 10. Phase diagrams obtained from the numerical solutions of the mean-field equations for a V(3:2) lattice with (a) neutral bias, (b) bias on only upstream segments, $\sigma^A = [0.1, 0.3, 0.6]$, (c) bias on only downstream segments, $\sigma^B = [0.25, 0.75]$, and (d) bias on both upstream and downstream segments, $\sigma^A = [0.1, 0.3, 0.6]$ and $\sigma^B = [0.25, 0.75]$.

Panel (b), with biases on the upstream segments ($\sigma^A = [0.1, 0.3, 0.6]$) shows that the area previously occupied by the 3HD:2MC phase in panel (a), is now by a 3HD:2LD phase, because particles on the upstream segments can less easily enter into the junction, and as the current entering the junction reduces, the density downstream the junction, on B segments, reduces too, causing them to be in a LD phase.

For different values of α, decreasing β induces a sequence of distinct phase transitions corresponding to the progressive filling of the lattice, starting from the downstream segments. For smaller values of α, the upstream segments get filled in a stepwise manner, with the unfavoured ones (low σ_i^A) being filled first. Thus, the effect of the bias is more noticeable as the entrance rate α is lower.

For different values of β, when increasing α, we observe that, while for high values of β (ca. $\beta > 0.44$), only the upstream segments get filled, for lower values of β (ca. $\beta < 0.44$), depending on the value of σ_i^A, the order in which upstream and downstream segments get filled is intricate. Yet, again, the most unfavoured ($\sigma_i^A = 0.1$) upstream segment is filled first and the most favoured one ($\sigma_i^A = 0.6$) last.

Panel (c), with biases on the downstream segments ($\sigma^B = [0.25, 0.75]$), shows that the area previously occupied by the 3HD:2MC phase in panel (a), is now by a 3HD:LD.MC phase, where the B segment with the lower bias goes to the LD phase, because particles from the junction cannot easily enter it.

For different values of α, decreasing β leads to a progressive filling of the lattice, starting with the most favoured downstream segment ($\sigma_j^B = 0.75$). This segment consequently enters either a HD or a MC phase, while the least favoured downstream segment ($\sigma_j^B = 0.25$) remains in a LD phase. A similar behaviour is observed for different values of β when increasing α.

Interestingly, for both panels (b) and (c), certain phase transitions involve Shock Phases with a Domain Wall that can be located in both upstream and downstream segments, which is consistent with previous observations [43].

In panel (d), as compared to panel (a) with neutral bias, the presence of a bias in all five segments gives rise to ten new phases in addition to the 3HD:2HD and 3LD:2LD phases. These new phases appear as a result of the distribution of the biases, such that upstream and downstream segments are distinct amongst themselves, and therefore get filled/emptied in a stepwise manner, reflected by complex combinations of phases, typically for intermediate values of α and β. Noticeably, the complexity of the phase diagram bursts, and is far more intricate than the simple overlay of the panels (b) and (c).

5.3.4. *Lattices with* $\lambda < 1$

The phase diagrams for a V(2:3) lattice (see Fig. F.14) can be derived from those shown in Fig. 10 for a V(3:2) lattice by particle–hole symmetry, exchanging upstream and downstream segments, α and β, and LD and HD phases. Consequently, all qualitative conclusions directly extend to this case. The impact of the distribution of either upstream or downstream segment biases on the junction current, can be quantified by the bottleneck coefficient (θ), which reveals that the bias of the upstream segments has a stronger effect than the one of the downstream ones for the studied V(2:3) lattice (see Appendix E). We can explain this by the fact that for an asymmetric lattice with neutral bias, the MC phase appears on the side of the junction with the lower number of segments, which is hence most impacted by the reduction of current.

6. Conclusion

Transport along complex one-dimensional lattices is widely prevalent in the real world, on a variety of scales, ranging from cellular cytoskeletal transport to nationwide road maps. These large and entangled networks, typically involve junctions where several tracks intersect and moving agents obey complex kinetic rules. The Totally Asymmetric Exclusion Process (TASEP) has initially been formulated for a single segment, and despite its many extensions, the study of Multiple-Input-Multiple-Output (MIMO) TASEP junctions with complex kinetic rules involving absorption, pumping, and biases remains a mathematical challenge calling for numerical approaches. In this study, we develop an innovative method involving formulating the combinatorial explosion of the phases on the lattice in the form of a matrix, as well as solving the conservation of the mean-field current at the junction using Constrained Optimisation, supplemented with stochastic simulations following a Gillespie algorithm.

Our results show that lattices with the same ratio of the number of upstream to downstream segments ($\lambda = \frac{m}{n}$) have the same phase diagrams, in the absence of a bottleneck effect and with neutral bias. Under these conditions, utilising particle–hole symmetry, it is also possible to deduce the phase diagrams for lattices related by $\lambda_2 = \frac{1}{\lambda_1}$. For segments with neutral bias, the bottleneck effect arises if either one of the three following conditions is satisfied: $\mu, \nu < \psi$ or $\mu \leq \mu^*$ or $\nu \leq \nu^*$. Here, μ^* and ν^* are lower thresholds of the absorption and pumping rates, respectively, below which the bottleneck effect appears, irrespective of the values of the other parameters. The bottleneck effect also arises for $\mu^* < \mu < \psi$ and $\nu > \psi$ in case ν is not high enough to compensate for the low absorption rate (μ) (and *vice versa*), or if a bias is introduced at the junction.

Depending on the fixed values of the absorption and pumping rates, increasing the number of upstream (m) or downstream (n) segments reduces the bottleneck coefficient (θ), and increases the bottleneck effect, which impacts both the transport on the individual segments and at the junction site, leading to a reduction of the current. For symmetric lattices, if the bottleneck effect is caused by equally low absorption (μ) and pumping (ν) rates, the maximal current occurs for the junction density $\tilde{\rho} = \frac{1}{2}$, similar to the case without the bottleneck effect. However, if it arises when $\mu < \nu$ or $\mu > \nu$, the maximal current is observed when $\tilde{\rho} < \frac{1}{2}$ or $\tilde{\rho} > \frac{1}{2}$, respectively. Independent of the values of μ and ν, the current-density relation at the junction for a bottlenecked lattice is no longer quadratic throughout, but becomes piece-wise quasi-linear.

When introducing biases on either or both of the upstream and downstream segments, the phenomenology gets very complex. The number of new phases in the phase diagram bursts, and we observe that filling the lattice does not only depend on the rates at the junction (absorption, pumping, and biases), and the number of upstream (m) and downstream (n) segments, but also on the values of the entrance (α) and exit (β) rates at the boundaries of the overall lattice. Specifically, at intermediate values of α and β, the dynamics of transport becomes intricate, and segments upstream and downstream of the junction both get filled in a stepwise manner. As the biases reduce the current, it may lead to the disappearance of the MC phase. Furthermore, particle–hole symmetry, well-established for a simple TASEP segment, extends here as well, allowing us to recover the phase diagrams for lattices by exchanging upstream and downstream segments, α and β, and LD and HD phases.

This study establishes a new and original method based on numerical solving for deciphering transport at a MIMO junction. While it is illustrated with example lattices involving only up to 5 segments, for demonstration purposes, it should be reminded that the method is fully generic and allows right-away tackling MIMO junctions with any number of upstream and downstream segments, as well as freely-selected values for the kinetic parameters at the junction (absorption, pumping, and bias rates). The complexity of the MIMO junction that one can investigate with this method is, hence, only limited by the available computational resources. A natural future development for the method would be to extend it to entire networks, which are typically more realistic

representations of real-world systems, like vehicular traffic at multi-lane intersections, and data or material transport in branched infrastructures. On such highly complex structures, congestion management is crucial, and so, our detailed study of the bottleneck effect at the MIMO junction specifically paves the way towards these future and applied investigations.

CRediT authorship contribution statement

Asma Ben Janete: Writing – original draft, Visualization, Validation, Software, Methodology, Investigation, Formal analysis, Data curation, Writing – review & editing. **Partho Sakha De:** Writing – review & editing, Writing – original draft, Validation, Formal analysis. **Adélaïde Raguin:** Writing – review & editing, Writing – original draft, Validation, Supervision, Resources, Project administration, Funding acquisition, Formal analysis, Conceptualization.

Funding

This work was supported by the Deutsche Forschungsgemeinschaft (DFG) under Germany's Excellence Strategy EXC 2048/1, Project ID: 390686111. The scientific activities of the Bioeconomy Science Center were financially supported by the Ministry of Culture and Science within the framework of the NRW Strategieprojekt BioSC (No. 313/323-400-002 13), that funds the positions of PSD and ABJ in the framework of the PREDIG and OptiCellu projects. The position of AR was funded by the German federal and state programme Professorinnenprogramm III for female scientists and by the Deutsche Forschungsgemeinschaft (DFG, German Research Foundation) in the framework of EtransColi (Project number: 470067901) that she coordinates.

Declaration of competing interest

The authors declare that they have no conflict of interest.

Appendix A. Glossary

A.1. List of symbols

α	Particle entrance rate to TASEP lattice
β	Particle exit rate from TASEP lattice
γ	Particle jumping rate (if next site is available)
ρ	Average particle density in the lattice
J	Average particle current in the lattice
m	Number of upstream segments
n	Number of downstream segments
λ	Ratio $\frac{m}{n}$
A_i	ith segment upstream of junction
B_j	jth segment downstream of junction
β_{eff_i}	Effective exit rate of the ith upstream segment
α_{eff_j}	Effective entrance rate of the jth downstream segment
$\tilde{\rho}$	Particle density at the junction
$\tilde{J}$	Current at the junction site
$\tilde{J}_{max}$	Maximum Current at the junction site
$\tilde{\rho}_{\tilde{J}_{max}}$	Junction density corresponding to the maximum junction current
J_{A_i}	Particle current in the ith upstream segment
J_{B_j}	Particle current in the jth downstream segment
μ	Absorption rate into the junction
ν	Pumping rate out of the junction
μ^*	Lowest threshold of μ below which bottle neck effect cannot be avoided
ν^*	Lowest threshold of ν below which bottleneck effect cannot be avoided
θ	Percentage of Maximum possible current when there is no bottleneck effect
ψ	Lowest value fulfilling $\mu = \nu = \psi$ and $\theta = 100\%$
σ^A	Bias across the upstream segments
σ^B	Bias across the downstream segments
$std(\sigma^A)$	Standard deviation of σ^A
$std(\sigma^B)$	Standard deviation of σ^B

A.2. Abbreviations

TASEP: Totally Asymmetric Exclusion Process, MIMO: Multiple-Input-multiple-Output, MISO: Multiple-Input-Single-Output, HD: High Density, LD: Low Density, MC: Maximal Current, SP: Shock Phase, PCM: Phase Combination Matrix, CO: Constrained Optimisation.

Appendix B. A brief reminder of TASEP at junctions

TASEP along a single segment (of finite size L with $L \gg 1$) consists of the stochastic unidirectional movement of a gas of particles that interact as hard-spheres, such that two particles or more cannot simultaneously occupy the same site [30]. Particles enter on one side of the lattice with an entrance rate α, move forward in the bulk with a jumping rate γ, and quit it with an exit rate β. Under the mean-field assumption, the steady state values of the phase diagram, the density, and the current have been determined for each phase and are summarised in Table B.3 [19]. The mean-field hypothesis assumes the absence of correlation between subsequent sites, which implies that the average density (noted ρ) is homogeneous along the lattice, except in the Shock Phase for which a Low Density phase on the left side of the lattice co-exists with a High Density phase on its right side, thereby forming a Domain Wall that fluctuates through time along the lattice as a random walker. In mean-field, the current (noted J) can be expressed as a function of the bulk density as: $J = \rho(1-\rho)$ (see Fig. B.11).

Fig. B.11. A schematic representation of the Totally Asymmetric Simple Exclusion Process (TASEP) on a single segment. Particles enter on the left with entrance rate α from an infinite reservoir, step along the segment with excluded-volume interactions with a rate γ, and leave the segment on the right with exit rate β to an infinite reservoir.

Table B.3
Density phases for a TASEP segment with their corresponding boundary rate conditions, average densities, and currents values.

Density phase	Conditions	Average density	Current
Low Density (LD)	$\alpha < \frac{1}{2}$ $\alpha < \beta$	$\rho = \alpha$	$J = \alpha(1-\alpha)$
High Density (HD)	$\beta < \frac{1}{2}$ $\beta < \alpha$	$\rho = 1-\beta$	$J = \beta(1-\beta)$
Maximal Current (MC)	$\alpha > \frac{1}{2}$ $\beta > \frac{1}{2}$	$\rho = \frac{1}{2}$	$J = \frac{1}{4}$
Shock Phase (SP)	$\alpha = \beta$ $\alpha < \frac{1}{2}$	$\rho = \frac{1}{2}$	$J = \alpha(1-\alpha)$

To expand mean-field results to structures with junctions, following the approach by Pronina and Kolomeisky [30], for each ith segment upstream the junction (noted A_i), one should define an effective exit rate β_{eff_i} as a function of the density at the junction $\tilde{\rho}$, and analogously, for each jth segment downstream the junction (noted B_j), define an effective entrance rate α_{eff_j}. Thus, each branch of the structure can be considered independently as a standalone TASEP segment, with respective boundary rates, that is nonetheless connected to the other segments through the junction. Then, each combination of phases occurring on upstream and downstream segments, must fulfil current conservation at the junction (*i.e.* $\sum_i J_{A_i} = \sum_j J_{B_j}$), while ensuring that the associated conditions are respected by the boundary rates of the respective individual segments. This allows determining the phase diagram of branched lattices, which shows different phase boundaries as compared to that of a simple TASEP segment (see the example of threefold lattices in Fig. B.12) [24,25,30].

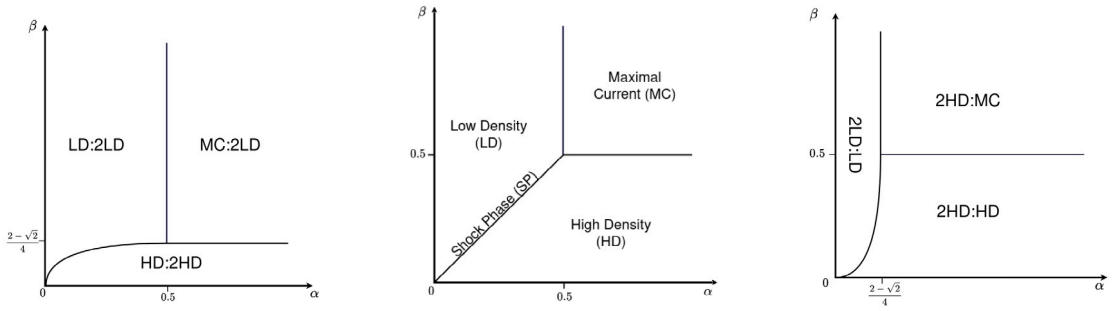

(a) V(1:2) lattice (b) One TASEP segment (c) V(2:1) lattice

Fig. B.12. The phase diagram of (a) a V(1:2) lattice, (b) a simple TASEP segment, and (c) a V(2:1) lattice in the steady state [25].

Appendix C. Calculation steps coefficients of mean-field expression for MIMO

C.1. A segments

Effective entrance and exit rates:
Entrance rate: α
Exit rate : $\mu\,\sigma_i^A\,(1-\tilde{\rho})$ with μ absorption rate into the junction and σ_i^A bias of segment A_i

C.1.1. If A_i has phase HD

Conditions on effective entrance and exit rates: $\beta_{eff_i} < \frac{1}{2} \quad \leftrightarrow \quad \mu\,\sigma_i^A\,(1-\tilde{\rho}) < \frac{1}{2}$ and $\beta_{eff_i} < \alpha \quad \leftrightarrow \quad \mu\,\sigma_i^A\,(1-\tilde{\rho}) < \alpha$
Current value: $J_{Ai} = \mu\,\sigma_i^A\,(1-\tilde{\rho})(1-\mu\,\sigma_i^A\,(1-\tilde{\rho})) \Leftrightarrow J_{Ai} = (\mu\,\sigma_i^A - \mu\,\sigma_i^A\,\tilde{\rho})(1-\mu\,\sigma_i^A + \mu\,\sigma_i^A\,\tilde{\rho}) \Leftrightarrow J_{Ai} = \mu\,\sigma_i^A - \mu\,\sigma_i^A\,\tilde{\rho} - (\mu\,\sigma_i^A)^2 + (\mu\,\sigma_i^A)^2\,\tilde{\rho} + (\mu\,\sigma_i^A)^2\,\tilde{\rho} - (\mu\,\sigma_i^A)^2\,\tilde{\rho}^2 \Leftrightarrow J_{Ai} = \tilde{\rho}^2\,(-(\mu\,\sigma_i^A)^2) + \tilde{\rho}\,(2\,(\mu\,\sigma_i^A)^2 - \mu\,\sigma_i^A) + (\mu\,\sigma_i^A - (\mu\,\sigma_i^A)^2)$
For the equation of current conservation: $a_{Ai} = -(\mu\,\sigma_i^A)^2 \;\; b_{Ai} = 2\,(\mu\,\sigma_i^A)^2 - \mu\,\sigma_i^A \;\; c_{Ai} = \mu\,\sigma_i^A - (\mu\,\sigma_i^A)^2$

C.1.2. If A_i has phase LD

Conditions on effective entrance and exit rates: $\alpha < \frac{1}{2}\;\; \alpha < \beta_{eff_i} \quad \leftrightarrow \quad \alpha < \mu\,\sigma_i^A\,(1-\tilde{\rho})$
Current value: $J_{Ai} = \alpha\,(1-\alpha)$
For the equation of current conservation: $a_{Ai} = 0 \;\; b_{Ai} = 0 \;\; c_{Ai} = \alpha\,(1-\alpha)$

C.1.3. If A_i has phase MC

Conditions on effective entrance and exit rates: $\alpha > \frac{1}{2}\;\; \beta_{eff_i} > \frac{1}{2} \quad \leftrightarrow \quad \mu\,\sigma_i^A\,(1-\tilde{\rho}) > \frac{1}{2}$
Current value: $J_{Ai} = \frac{1}{4}$
For the equation of current conservation: $a_{Ai} = 0 \;\; b_{Ai} = 0 \;\; c_{Ai} = \frac{1}{4}$

C.1.4. If A_i has phase SP

Conditions on effective entrance and exit rates: $\alpha < \frac{1}{2}\;\; \alpha = \beta_{eff_i} \quad \leftrightarrow \quad \alpha = \mu\,\sigma_i^A\,(1-\tilde{\rho}) \quad \leftrightarrow \quad \tilde{\rho} = 1 - \frac{\alpha}{\mu\,\sigma_i^A}$
Current value: $J_{Ai} = \alpha\,(1-\alpha) = \mu\,\sigma_i^A\,(1-\tilde{\rho})(1-\mu\,\sigma_i^A\,(1-\tilde{\rho}))$
For the equation of current conservation: $a_{Ai} = 0 \;\; b_{Ai} = 0 \;\; c_{Ai} = \alpha\,(1-\alpha)$
Or: $a_{Ai} = -(\mu\,\sigma_i^A)^2 \;\; b_{Ai} = 2\,(\mu\,\sigma_i^A)^2 - \mu\,\sigma_i^A \;\; c_{Ai} = \mu\,\sigma_i^A - (\mu\,\sigma_i^A)^2$
NB:
$\forall\; i\,,\; l \; with \; i, l \in [1..m] \; and \; i \neq l\;\;,$ if A_i has density phase MC, A_l cannot have LD or SP because of contradictory constraints on α.

C.2. B segments

Effective entrance and exit rates:
Entrance rate: $\alpha_{eff_j} = \nu\,\sigma_j^B\,\tilde{\rho}$ with ν pumping rate out of the junction and σ_j^B bias of segment $B-j$
Exit rate: β

C.2.1. If B_j has phase HD

Conditions on effective entrance and exit rates: $\beta < \frac{1}{2}\ \beta < \alpha_{eff_j} \quad \leftrightarrow \quad \beta < \nu\,\sigma_j^B\,\tilde{\rho}$
Current value: $J_{Bj} = \beta\,(1-\beta)$
For the equation of current conservation: $a_{Bj} = 0\ b_{Bj} = 0\ c_{Bj} = \beta\,(1-\beta)$

C.2.2. If B_j has phase LD

Conditions on effective entrance and exit rates: $\alpha_{eff_j} < \frac{1}{2} \quad \leftrightarrow \quad \nu\,\sigma_j^B\,\tilde{\rho} < \frac{1}{2}\ \alpha_{eff_j} < \beta \quad \leftrightarrow \quad \nu\,\sigma_j^B\,\tilde{\rho} < \beta$
Current value: $J_{Bj} = \nu\,\sigma_j^B\,\tilde{\rho}\,(1-\nu\,\sigma_j^B\,\tilde{\rho})\ J_{Bj} = \nu\,\sigma_j^B\,\tilde{\rho} - (\nu\,\sigma_j^B)^2\,\tilde{\rho}^2$
For the equation of current conservation: $a_{Bj} = -(\nu\,\sigma_j^B)^2\ b_{Bj} = \nu\,\sigma_j^B\ c_{Bj} = 0$

C.2.3. If B_j has phase MC

Conditions on effective entrance and exit rates: $\beta > \frac{1}{2}\ \alpha_{eff_j} > \frac{1}{2} \quad \leftrightarrow \quad \nu\,\sigma_j^B\,\tilde{\rho} > \frac{1}{2}$
Current value: $J_{Bj} = \frac{1}{4}$
For the equation of current conservation: $a_{Bj} = 0\ b_{Bj} = 0\ c_{Bj} = \frac{1}{4}$

C.2.4. If B_j has phase SP

Conditions on effective entrance and exit rates: $\beta < \frac{1}{2}\ \beta = \alpha_{eff_j} \quad \leftrightarrow \quad \beta = \nu\,\sigma_j^B\,\tilde{\rho} \quad \leftrightarrow \quad \tilde{\rho} = \frac{\beta}{\nu\,\sigma_j^B}$
Current value: $J_{Bi} = \beta\,(1-\beta) = \nu\,\sigma_j^B\,\tilde{\rho} - (\nu\,\sigma_j^B)^2\,\tilde{\rho}^2$
For the equation of current conservation:
$a_{Bj} = 0$
$b_{Bj} = 0$
$c_{Bj} = \beta(1-\beta)$
Or:
$a_{Bj} = -(\nu\,\sigma_j^B)^2$
$b_{Bj} = \nu\,\sigma_j^B$
$c_{Bj} = 0$
NB:
$\forall\ j\ ,\ l\ with\ j,l \in [1..n]\ and\ i \neq l\ \ ,$ if B_j has density phase MC, B_l cannot have HD or SP because of contradictory constraints on β.

Appendix D. Calculations details for the bottleneck effect threshold parameter ψ

We want to calculate ψ for a V(m: n) lattice. ψ is the lowest value of absorption and pumping rates so that the MC phase occurs on the junction side with the lower number of segments. Thus, if $m < n$, the system is in the mMC:nLD phase. If $m = n$, the system is in mMC:nMC phase and if $m > n$, the system is the mHD:nMC phase. Let $a, b \in \mathbf{N}$ with $a > b$ such that $a = \max(m,n)$ and $b = \min(m,n)$. We know that V(a:b) and V(b:a) share the same value of ψ. We try to find an equation of ψ for V(a:b) and V(b:a) lattices. To begin we define the entrance and exit rates of the A and B segments:

- Entrance rate of A segments: $\alpha_A = \alpha$
- Exit rate of A segments: $\beta_A = (1-\tilde{\rho})\psi\frac{1}{a}$
- entrance rate of B segments: $\alpha_B = \tilde{\rho}\psi\frac{1}{b}$
- exit rate of B segments: $\beta_B = \beta$

aHD:bMC on V(a:b)
We denote $\tilde{\rho_1}$ as the density at the junction of V(a:b).
current conservation:
$a\psi\frac{1}{a}(1-\tilde{\rho_1})(1-\psi\frac{1}{a}(1-\tilde{\rho_1})) = b\frac{1}{4}$
$\psi(1-\tilde{\rho_1})(1-\frac{\psi}{a}(1-\tilde{\rho_1})) = \frac{b}{4}$

bMC:aLD on V(b:a)
We denote $\tilde{\rho_2}$ as the density at the junction of V(b:a).
current conservation:
$b\frac{1}{4} = a\psi\frac{1}{a}\tilde{\rho_2}(1-\psi\frac{1}{a}\tilde{\rho_2})$
$\frac{b}{4} = \psi\tilde{\rho_2}(1-\frac{\psi}{a}\tilde{\rho_2})$

Applying the particle–hole symmetry, we know that the density of particles on V(a:b) equals the density of holes in V(b:a), i.e. $\tilde{\rho_1} = 1 - \tilde{\rho_2}$. We have here 2 unknowns, ψ and $\tilde{\rho_2}$ and both equations of the current conservation result in one namely:

$$\psi^2 \tilde{\rho_2}^2 \frac{1}{a} - \psi \tilde{\rho_2} + \frac{b}{4} = 0$$

$$\Delta_\psi = \tilde{\rho_2}^2 - 4\frac{b}{4}\frac{1}{a}\tilde{\rho_2}^2 \quad = \tilde{\rho_2}^2(1 - \frac{b}{a})\ \psi = \frac{\tilde{\rho_2}(1-\sqrt{1-\frac{b}{a}})}{2\frac{\tilde{\rho_2}^2}{a}} \quad = \frac{a(1-\sqrt{1-\frac{b}{a}})}{2\tilde{\rho_2}} \text{ or } \psi = \frac{\tilde{\rho_2}(1+\sqrt{1-\frac{b}{a}})}{2\frac{\tilde{\rho_2}^2}{a}} \quad = \frac{a(1+\sqrt{1-\frac{b}{a}})}{2\tilde{\rho_2}}$$

Since, ψ is by definition the lowest positive value of both pumping and absorption that ensures that $\theta = 100\%$, we select the solution: $\psi = \frac{a(1-\sqrt{1-\frac{b}{a}})}{2\tilde{\rho_2}}$.

For lattices with $m > n$, we substitute $\tilde{\rho_2}$ with $1 - \tilde{\rho_1}$, such that the equation reads as: $\psi = \frac{a(1-\sqrt{1-\frac{b}{a}})}{2(1-\tilde{\rho_1})}$.

Appendix E. Impact of the bias on the bottleneck effect

Fig. E.13 shows the bottleneck coefficient (θ) depending on the standard deviation amongst the biases of either upstream (A) or downstream (B) segments, σ_i^A and σ_j^B, respectively. The standard deviation of the bias is defined as $std(\sigma^x) = \sqrt{\frac{1}{y}\sum\left(\sigma_i^x - \frac{\sum\sigma_i^x}{y}\right)^2}$, where $x = A, y = m$ for the upstream segments and $x = B, y = n$ for the downstream ones, respectively. The lattice is a V(2:3) with $\mu = \nu = \psi = 1.64$, such that with neutral bias amongst the segments, there is no bottleneck effect ($\theta = 100\%$), as can be seen on the top-left. We observe that when either of the upstream or downstream segments are biased, there is a monotonic decrease of θ with increasing standard deviation of the biases, which is consistent with results found for closed systems [24,26].

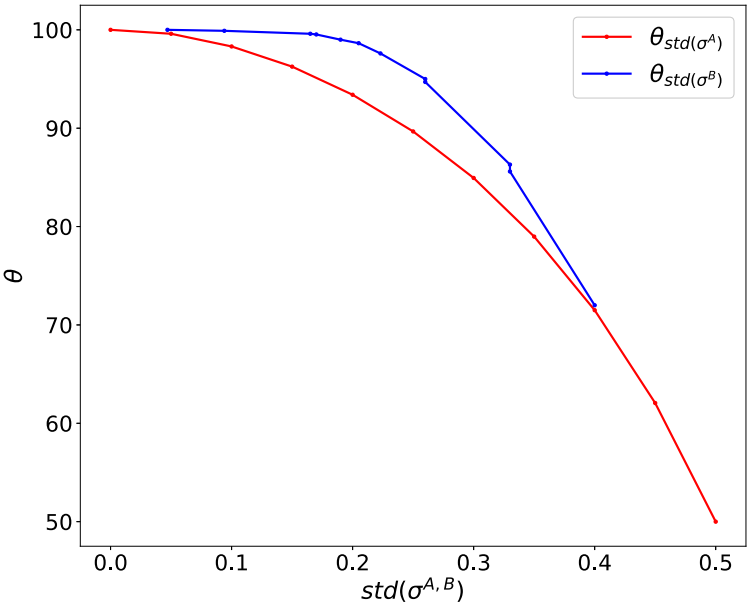

Fig. E.13. Bottleneck coefficient (θ) *versus* the standard deviation of the bias ($std(\sigma^{A,B})$) obtained from the numerical solutions of the mean-field equations of a V(2:3) lattice, with $\mu = \nu = \psi = 1.64$, the lowest value ensuring $\theta = 100\%$, with neutral bias. Either the upstream (A) or the downstream (B) segments are biased, while the segments opposite the junction remain neutrally biased.

For the lattice considered, a V(2:3), the decrease of θ with the increase in the standard deviation of the biases is stronger for the upstream segments than for the downstream ones. For a V(2:3) lattice with $\mu = \nu = \psi = 1.64$, in the absence of a bias (thus without the bottleneck effect) the upstream segments accommodate a MC phase and the downstream segments are in the LD phase. Thus, the segments accommodating the MC phase, here the upstream ones, are those most impacted by the bottleneck effect.

Appendix F. Lattices with $\lambda < 1$

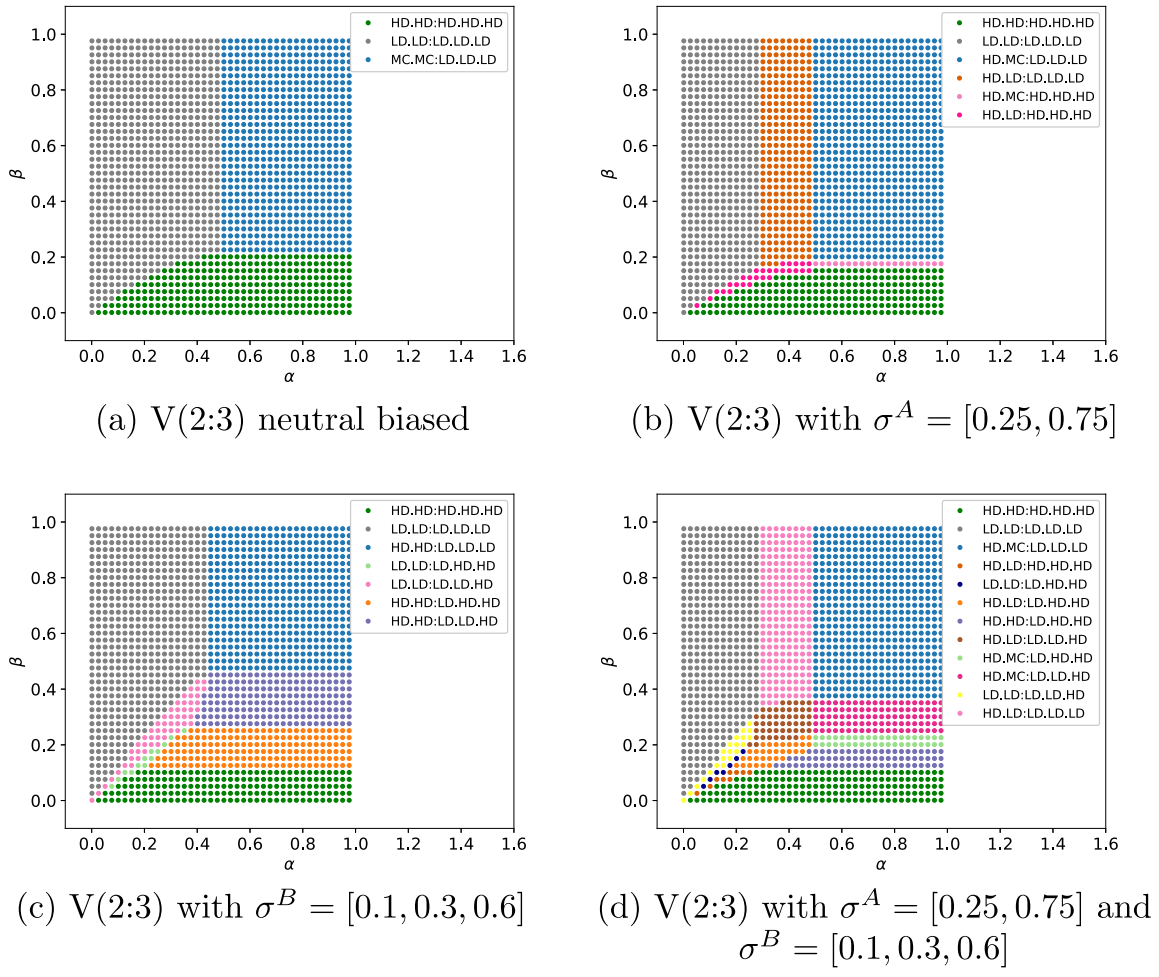

(a) V(2:3) neutral biased

(b) V(2:3) with $\sigma^A = [0.25, 0.75]$

(c) V(2:3) with $\sigma^B = [0.1, 0.3, 0.6]$

(d) V(2:3) with $\sigma^A = [0.25, 0.75]$ and $\sigma^B = [0.1, 0.3, 0.6]$

Fig. F.14. Phase diagrams obtained from the numerical solutions of the mean-field equations for a V(2:3) lattice with (a) neutral bias, (b) bias on only upstream segments, $\sigma^A = [0.25, 0.75]$, (c) bias on only downstream segments, $\sigma^B = [0.1, 0.3, 0.6]$, and (d) bias on both upstream and downstream segments, $\sigma^A = [0.25, 0.75]$ and $\sigma^B = [0.1, 0.3, 0.6]$.

Data availability

The simulation and analysis codes of the model, together with the scripts for reproducing the figures, are provided in the GitLab repository accessible via https://gitlab.com/asben100/complex-tasep-mimo-junction.

References

[1] Ankita Gupta, et al., Modelling of transport processes: Theory and simulations, MethodsX 10 (2023) 101966.
[2] Carolyn T. MacDonald, Julian H. Gibbs, Allen C. Pipkin, Kinetics of biopolymerization on nucleic acid templates, Biopolym.: Orig. Res. Biomol. 6 (1) (1968) 1–25.
[3] R.K.P. Zia, J.J. Dong, B. Schmittmann, Modeling translation in protein synthesis with TASEP: A tutorial and recent developments, J. Stat. Phys. 144 (2) (2011) 405–428, http://dx.doi.org/10.1007/s10955-011-0183-1, [https://doi.org/10.1007%2Fs10955-011-0183-1].
[4] L. Ciandrini, I. Stansfield, M.C. Romano, Role of the particle's stepping cycle in an asymmetric exclusion process: A model of mRNA translation, Phys. Rev. E 81 (5) (2010) http://dx.doi.org/10.1103/physreve.81.051904.
[5] Luca Ciandrini, Ian Stansfield, M. Carmen Romano, Ribosome traffic on mRNAs maps to gene ontology: Genome-wide quantification of translation initiation rates and polysome size regulation, in: Andrey Rzhetsky (Ed.), PLoS Comput. Biol. 9 (1) (2013) e1002866, http://dx.doi.org/10.1371/journal.pcbi.1002866.
[6] Debashish Chowdhury, et al., From CA to gene expression: Machines and mechanisms, in: Hiroshi Umeo, Shin Morishita, Katsuhiro Nishinari, Toshihiko Komatsuzaki, Stefania Bandini (Eds.), Cellular Automata, Springer Berlin Heidelberg, Berlin, Heidelberg, 2008, pp. 1–10.
[7] C. Appert-Rolland, M. Ebbinghaus, L. Santen, Intracellular transport driven by cytoskeletal motors: General mechanisms and defects, Phys. Rep. 593 (2015) 1–59, http://dx.doi.org/10.1016/j.physrep.2015.07.001, [https://doi.org/10.1016%2Fj.physrep.2015.07.001].

[8] Luiza V.F. Gomes, Anatoly B. Kolomeisky, Dynamics of relaxation to a stationary state for interacting molecular motors, J. Phys. A 51 (1) (2017) 015601.
[9] Izaak Neri, Norbert Kern, Andrea Parmeggiani, Exclusion processes on networks as models for cytoskeletal transport, New J. Phys. 15 (8) (2013) 085005, http://dx.doi.org/10.1088/1367-2630/15/8/085005.
[10] Izaak Neri, Norbert Kern, Andrea Parmeggiani, Modeling cytoskeletal traffic: An interplay between passive diffusion and active transport, Phys. Rev. Lett. 110 (2013) 098102, http://dx.doi.org/10.1103/PhysRevLett.110.098102, URL https://link.aps.org/doi/10.1103/PhysRevLett.110.098102.
[11] Luca Ciandrini, et al., Motor protein traffic regulation by supply–demand balance of resources, Phys. Biol. 11 (5) (2014) 056006, http://dx.doi.org/10.1088/1478-3975/11/5/056006.
[12] Luca Ciandrini, M. Carmen Romano, Andrea Parmeggiani, Stepping and crowding of molecular motors: Statistical kinetics from an exclusion process perspective, Biophys. J. 107 (5) (2014) 1176–1184, http://dx.doi.org/10.1016/j.bpj.2014.07.012.
[13] Daichi Yanagisawa, Akiyasu Tomoeda, Katsuhiro Nishinari, Influence of Rhythm and velocity variance on pedestrian flow, in: Ulrich Weidmann, Uwe Kirsch, Michael Schreckenberg (Eds.), Pedestrian and Evacuation Dynamics 2012, Springer International Publishing, Cham, 2014, pp. 1291–1303.
[14] H. Hilhorst, Cecile Appert-Rolland, A multi-lane TASEP model for crossing pedestrian traffic flows, J. Stat. Mechanics-Theory Exp. - J STAT MECH-THEORY EXP 2012 (2012) http://dx.doi.org/10.1088/1742-5468/2012/06/P06009.
[15] Claudio Feliciani, Measurement and Numerical Modeling of Pedestrian Flows (Ph.D. thesis), The University of Tokyo, 2017.
[16] Kai Nagel, Particle hopping models and traffic flow theory, Phys. Rev. E 53 (5) (1996) 4655–4672, http://dx.doi.org/10.1103/physreve.53.4655, [https://doi.org/10.1103%2Fphysreve.53.4655].
[17] Valentin Anfray, Alexandre Nicolas, Non-monotonic flow variations in a TASEP-based traffic model featuring cars searching for parking, 2023, arXiv:2309.12698.
[18] Rob van Nes, Gerard de Jong, Chapter four - transport models, in: Niek Mouter (Ed.), Standard Transport Appraisal Methods, in: Advances in Transport Policy and Planning, vol. 6, Academic Press, 2020, pp. 101–128, http://dx.doi.org/10.1016/bs.atpp.2020.08.001, URL https://www.sciencedirect.com/science/article/pii/S2543000920300342.
[19] Bernard Derrida, Eytan Domany, David Mukamel, An exact solution of a one-dimensional asymmetric exclusion model with open boundaries, J. Stat. Phys. 69 (1992) 667–687.
[20] Anatoly B Kolomeisky, et al., Phase diagram of one-dimensional driven lattice gases with open boundaries, J. Phys. A: Math. Gen. 31 (33) (1998) 6911.
[21] Anatoly B. Kolomeisky, Asymmetric simple exclusion model with local inhomogeneity, J. Phys. A: Math. Gen. 31 (4) (1998) 1153.
[22] Jordan Brankov, Nina Pesheva, Nadezhda Bunzarova, Totally asymmetric exclusion process on chains with a double-chain section in the middle: Computer simulations and a simple theory, Phys. Rev. E 69 (6) (2004) 066128.
[23] M. Ebrahim Foulaadvand, Philipp Maass, Phase transitions and optimal transport in stochastic roundabout traffic, Phys. Rev. E 94 (1) (2016) 012304.
[24] Ben Embley, Andrea Parmeggiani, Norbert Kern, Understanding totally asymmetric simple-exclusion-process transport on networks: Generic analysis via effective rates and explicit vertices, Phys. Rev. E 80 (4) (2009) 041128.
[25] Adélaïde Raguin, Norbert Kern, Andrea Parmeggiani, Stochastic modelling of collective motor protein transport through a crossing of microtubules, J. Theoret. Biol. 505 (2020) 110370.
[26] Adélaïde Raguin, Andrea Parmeggiani, Norbert Kern, Role of network junctions for the totally asymmetric simple exclusion process, Phys. Rev. E 88 (4) (2013) 042104.
[27] Štefan Bálint, et al., Correlative live-cell and superresolution microscopy reveals cargo transport dynamics at microtubule intersections, Proc. Natl. Acad. Sci. 110 (9) (2013) 3375–3380.
[28] Katherine Luby-Phelps, Cytoarchitecture and physical properties of cytoplasm: volume, viscosity, diffusion, intracellular surface area, Int. Rev. Cytol. 192 (1999) 189–221.
[29] Ankita Gupta, Arvind Kumar Gupta, Exclusion processes on a roundabout traffic model with constrained resources, Phys. Rev. E 108 (6) (2023) 064116.
[30] Ekaterina Pronina, Anatoly B. Kolomeisky, Theoretical investigation of totally asymmetric exclusion processes on lattices with junctions, J. Stat. Mech. Theory Exp. 2005 (07) (2005) P07010.
[31] Akriti Jindal, Arvind Kumar Gupta, Effect of local dissociation on symmetry breaking in exclusion model constituted by bridge lane and input-output TASEPs, Chaos Solitons Fractals 152 (2021) 111354.
[32] Ruili Wang, Mingzhe Liu, Rui Jiang, Theoretical investigation of synchronous totally asymmetric exclusion processes on lattices with multiple-input–single-output junctions, Phys. Rev. E 77 (5) (2008) 051108.
[33] Mingzhe Liu, Ruili Wang, Asymmetric exclusion processes on m-input n-output junctions with parallel update, Phys. A 388 (19) (2009) 4068–4074.
[34] Li Shao-Da, Liu Ming-Zhe, Pei Xiang-Jun, Totally asymmetric exclusion processes at constrained m-input-n-output junction points, 2013.
[35] Tripti Midha, Anatoly B. Kolomeisky, Arvind Kumar Gupta, Theoretical study of network junction models for totally asymmetric exclusion processes with interacting particles, J. Stat. Mech. Theory Exp. 2019 (8) (2019) 083202.
[36] Ankita Gupta, Arvind Kumar Gupta, Particle creation and annihilation in an exclusion process on networks, J. Phys. A 55 (10) (2022) 105001.
[37] Ankita Gupta, Arvind Kumar Gupta, Non-equilibrium processes in an unconserved network model with limited resources, Eur. Phys. J. Plus 138 (2) (2023) 108.
[38] Jennifer L Ross, et al., Kinesin and dynein-dynactin at intersecting microtubules: motor density affects dynein function, Biophys. J. 94 (8) (2008) 3115–3125.
[39] Stephanie K Deeb, et al., The ability of the kinesin-2 heterodimer KIF3AC to navigate microtubule networks is provided by the KIF3A motor domain, J. Biol. Chem. 294 (52) (2019) 20070–20083.
[40] Dimitri P. Bertsekas, Constrained Optimization and Lagrange Multiplier Methods, Academic Press, 2014.
[41] Daniel T. Gillespie, A general method for numerically simulating the stochastic time evolution of coupled chemical reactions, J. Comput. Phys. 22 (4) (1976) 403–434, http://dx.doi.org/10.1016/0021-9991(76)90041-3, URL https://www.sciencedirect.com/science/article/pii/0021999176900413.
[42] Daniel T. Gillespie, Exact stochastic simulation of coupled chemical reactions, J. Phys. Chem. 81 (25) (1977) 2340–2361, http://dx.doi.org/10.1021/j100540a008.
[43] Ekaterina Pronina, Anatoly B. Kolomeisky, Theoretical investigation of totally asymmetric exclusion processes on lattices with junctions, J. Stat. Mech. Theory Exp. 2005 (07) (2005) P07010, http://dx.doi.org/10.1088/1742-5468/2005/07/P07010.